

Battery thermal-health jointly concerned charging scheduling for Solar PV penetrated Energy-Transportation Nexus: a DRL-based approach empowered by a Cyber-Physical system

Xuyang Zhao¹, Hongwen He^{1*}, Jianwei Li¹, Zhongbao Wei¹, Ruchen Huang¹, Hongwei Yue¹

¹ National Engineering Laboratory for Electric Vehicles, Beijing Institute of Technology, Beijing, China

(*Corresponding Author: hwhebit@bit.edu.cn)

ABSTRACT

Using effective vehicle-to-grid (V2G) strategies, the onboard batteries in grid-connected electric vehicles (GEVs) can be leveraged to alleviate the impact of solar photovoltaic (PV) systems and provide grid support. Nevertheless, the abuse of batteries during V2G is inevitable owing to balancing the fluctuation of solar power while ensuring charging effectiveness, resulting in risks on battery rapid degradation and thermal safety. Regarding this, a multi-physics-constrained charging scheduling strategy is proposed in this study, enabled by a novel deep reinforcement learning (DRL) technique to mitigate solar PV impact while minimize the expected customer's charging cost, including energy cost and battery aging cost as well as satisfying the customer service quality and battery operation safety constraints. The proposed strategy is further performed within a cyber physical system-based framework, where the complicated training is carried out in the cloud, while the trained low-complexity policy is executed in the onboard controller to mitigate high computing burden. The effectiveness of the proposed strategy is verified by hardware-in-Loop tests and practical battery charging/discharging experiments combined by a real distribution system in Australia.

Keywords: renewable energy resources, grid-connected electric vehicles (GEVs), deep reinforcement learning (DRL), battery health management, thermal safety

1. INTRODUCTION

Electric vehicles (EVs) represent a promising solution that can alleviate the environmental impacts with fossil fuel transportation, among which plug-in EVs (PEVs) have gained widespread popularity for home mobility due to their convenient charging methods and cost-effective usage[1]. However, uncontrolled residential charging of PEVs may violate the operational constraints of power distribution systems. More significantly, with the rapid growth in the penetration rate of domestic renewable energy generation equipment such as solar photovoltaic

(PV), the volatile and time-varying power generation also pose great challenges to the stability constraints of power distribution systems with PEVs. For this issue, an effective vehicle-to-grid (V2G) power scheduling strategy is vital not only for the smooth operation of electric grid but for PEVs charging performance.

Numerous V2G management techniques have been developed in previous studies, which can be broadly divided into two categories. In the first category, the heuristic rules or fuzzy logic are adopted for PEVs charging/discharging scheduling for specific objectives[2], such as maximizing the load factor of feeders, minimizing customers' energy cost and peak shaving[3]. These methods have fundamental scheduling function but are typically empirical, thus failing to take comprehensive objectives into account. Correspondingly, a more common approach is the methods incorporating optimization algorithms and power system models to make planning on energy scheduling based on single or multiple objectives. Compared with the rule-based strategies, optimization-based methods can use the related algorithms to achieve the multiple conflicting objectives in scheduling, including power variation of grid, charging demand and battery degradation of PEVs [4, 5].

The utilization of emerging artificial intelligence (AI) and cloud computing technologies to achieve V2G scheduling represents a current trend. Particularly, reinforcement learning algorithms exhibit strong multi-objective optimization performance while avoiding the complex models in optimization-based methods above, thereby have been applied for various optimization problems[6]. More significantly, Cyber Physical System (CPS) is a cutting-edge technology that fuses computational processes (cyber layer) with the tangible world (physical layer) through integrated computation, control, and communication technology, which provides an effective framework basis for AI algorithms establishment and strategy deployment[7]. Therefore, the V2G scheduling strategy proposed in this study is established based on the CPS framework, as shown in

Fig.1. In cyber layer, a wealth of diverse and heterogeneous multi-source data is meticulously fused and processed for the intelligent algorithm training. More specifically, a PEV consists of the Lithium-ion battery (LIB) system and a battery management system (BMS). On this basis, the operating data, including current, terminal voltage and temperature of a LIB, can be collected and uploaded to the database in cyber-layer. Additionally, the database also receives and stores the battery test data as well as the key information of Solar PVs and grids. The intelligent models in computing platform are trained using the data in database to obtain optimal strategy comprehensively considering the costs, customer dissatisfaction, power fluctuation and LIB thermal safety. The details are introduced as follows.

2. MODELING FOR THE PHYSICAL LAYER

2.1 Energy-Transportation Nexus Configuration

As shown in Fig.1, in a PEV-PV cluster, there is a PEV

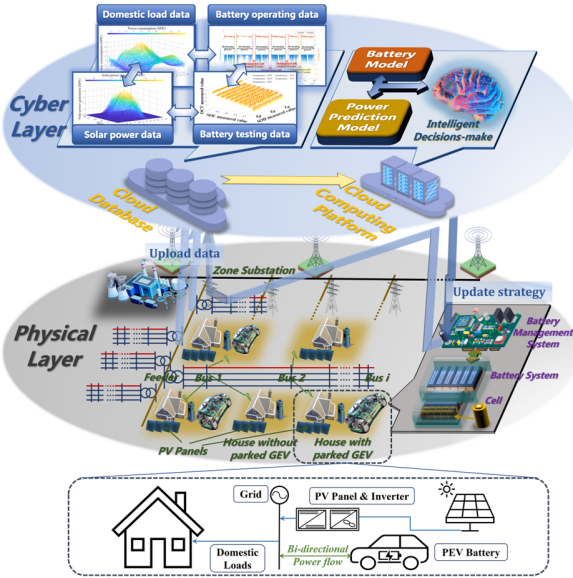


Fig. 1 Overall cyber-physical system framework

connected to a point of common coupling (PCC) with a PV system, household loads and the distribution grid. Solar energy can be converted to electricity power by PVs for domestic loads and PEVs charging. Obviously, PEVs connected to the feeder can bring considerable benefits for the whole feeder and upstream network in terms of voltage rise mitigation. Regarding this, a wise charging/discharging strategy is necessary.

2.2 Customer service quality evaluation

In this study, two factors are taken into account for the customer dissatisfaction assessment: 1. The time spent on waiting before the target battery SOC level is reached; 2. SOC in each time step. More specifically, as shown in Fig. 2, the PEV with a LIB at the initial SOC level

reaches home at T_{rh} . When charged with its maximum rate without control, the LIB spends L_{cd} hours to attain the target SOC. If the charging duration exceeds L_{cd} , there will be dissatisfaction among customers, and the degree relies on the battery SOC after $T_{rh}+L_{cd}$ and the waiting time t . $T_{rh}-T_{hd}$ is the dwelling time. $T_{hd}-t$ is the remaining time for charging, and L_d-L_{cd} is the total charging time that can be controlled. Then the dissatisfaction can be evaluated according to the Kano's model as follows[8]:

$$P_{dissa} = \sum_{t=T_{rh}+L_{cd}}^{T_{hd}} P_{dissa,t} = \sum_{t=T_{rh}+L_{cd}}^{T_{hd}} a \times \exp(-x_t) - b \quad (1)$$

where

$$x_t = \begin{cases} \tau_t \times (1 - \zeta_t), & \text{if } \sigma_t < \sigma^{des} \\ 1, & \text{if } \sigma_t = \sigma^{des} \end{cases} \quad (2)$$

$$\tau_t = \frac{T_{hd} - t}{L_d - L_{cd}} \quad (3)$$

$$\zeta_t = \frac{\sigma^{des} - \sigma_t}{\sigma^{des} - \sigma^{min}} \quad (4)$$

$$L_{cd} = \frac{(\sigma^{des} - \sigma^{ini})\beta}{P_{G2V,max} \eta_{G2V}} \quad (5)$$

In Eq. (4), $\sigma^{des} - \sigma_t$ is the SOC remaining for reaching the desired SOC. τ_t reflects how well the customer's requirements are met at t , considering the waiting time. $(1 - \zeta_t)$ reflects how well the customer's requirements are met at t . When $\tau_t = 1$ and $\zeta_t = 0$, the customer is completely satisfied. If at $T_{rh}+L_{cd}$, the battery reaches σ^{des} and the customer is completely satisfied. If not, the dissatisfaction determined by Eq. (1) is imposed. The energy needed at the arrival time to reach the target SOC can be obtained as $(\sigma^{des} - \sigma^{ini})\beta$ in Eq. (5).

2.3 Battery electrothermal-aging Modeling

Improper charging/ discharging methods may have

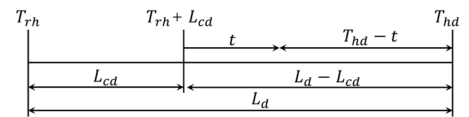


Fig. 2 Incorporated timing parameters in scheduling

an adverse effect on battery health and thermal safety. Therefore, as shown in Fig. 3, an electrothermal-aging

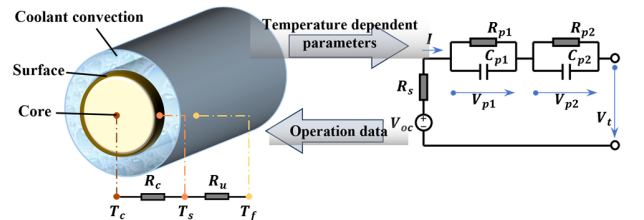


Fig. 3 Schematic of the electro-thermal model

model is established to accurately estimate the real-time state of LIBs and subsequently obtain the optimal charging/discharging mode, in which the open-circuit voltage is usually a nonlinear function of SOC[9]:

$$V_t(t) = V_{OCV}(t, SOC) + V_{RC1}(t) + V_{RC2}(t) + I(t)R_s(t) \quad (6)$$

where V_t and I are the terminal voltage and load current, respectively. SOC can be obtained by coulomb counting:

$$\frac{dSOC(t)}{dt} = \frac{I(t)}{3600C_{bat}} \quad (7)$$

where C_{bat} is the nominal battery capacity.

In the two RC branches adopted in this study, there is voltage drop across the RC branches and the ohmic resistance R_s , which can be described as:

$$\frac{dV_{RC1}(t)}{dt} = -\frac{V_{RC1}(t)}{R_{RC1}(t)C_{RC1}(t)} + \frac{I(t)}{C_{RC1}(t)} \quad (8)$$

$$\frac{dV_{RC2}(t)}{dt} = -\frac{V_{RC2}(t)}{R_{RC2}(t)C_{RC2}(t)} + \frac{I(t)}{C_{RC2}(t)} \quad (9)$$

where R_{RC1} and R_{RC2} are the equivalent resistance while C_{RC1} and C_{RC2} are the capacitance. And V_{RC1} and V_{RC2} are the polarization voltage across the RC branches.

The lumped thermal dynamics of a cylindrical battery cell can be calculated using the model in Fig.3 as[9]:

$$C_s \frac{dT_s(t)}{dt} = \frac{T_f(t) - T_s(t)}{R_u} + 2 \frac{T_a(t) - T_s(t)}{R_c} \quad (10)$$

$$\frac{dT_a(t)}{dt} = \left(\frac{C_s - C_c}{R_c C_c C_s} - \frac{1}{2R_u C_s} \right) T_s(t) + \frac{C_c - C_s}{R_c C_c C_s} T_a(t) + \frac{H(t)}{2C_c} + \frac{T_f}{2R_u C_s} \quad (11)$$

where T_s and T_f represent the temperature on the surface of cell and the surrounding ambient temperature, T_a is the average value. R_c and R_u represent the heat conduction resistance and the thermal resistance. C_c and C_s represent the heat capacity of the core and the surface. H is the heat producing rate and can be calculated as:

$$H(t) = I(t)[V_{RC1}(t) + V_{RC2}(t) + R_s(t)I(t) + (T_a(t) + 273)E_n(SOC, t)] \quad (12)$$

where E_n is the entropy change. The core temperature is:

$$T_c(t) = 2T_a(t) - T_s(t) \quad (13)$$

In this study, an energy-throughput-based model is established to estimate battery aging state. The state-of-health (SOH) of a LIB cell can be calculated by[10]:

$$\frac{dSOH(t)}{dt} = -\frac{1}{2N(c, T_a)C_{bat}} \int_0^t |P_i(\tau)| d\tau \quad (14)$$

where N represents the cycle number before end of life (EOL). Obviously, the two main factors affecting N are C-rate (c) and cell temperature (T_a). And there is capacity loss ΔC_{bat} with respect to the initial capacity, which can be estimated based on Arrhenius equation:

$$\Delta C_{bat} = B(c) \cdot \exp\left(\frac{-E_a(c)}{R \cdot T_a}\right) \cdot A(c)^{-\gamma} \quad (15)$$

where $B(c)$ is the pre-exponential factor which depends on the C-rate. And the $B(c)$ values corresponding to different c values. Moreover, R is the ideal gas constant which equals to $8.31J/mol \cdot K$ while the total throughput $A(c)$ is a function of C-rate, $E_a(c)$ is the activation energy:

$$E_a(c) = (31700 - 370.3 \cdot c) J / mol \quad (16)$$

As mentioned above, a battery reaches EOL when the available capacity decreases by 20%. Then A and N can be obtained according to Eq. (9)-(17):

$$A(c, T_a) = \left[\frac{\Delta C_{bat}}{B(c) \cdot \exp\left(-\frac{E_a(c)}{R \cdot T_a}\right)} \right]^{1/\gamma} \quad (17)$$

$$N(c, T_a) = \frac{V_{oc} \cdot A(c, T_a)}{C_{bat}} \quad (18)$$

In this way, aging conditions under given charging/discharging current, ambient temperature and operation history can be finally obtained.

3. DRL-BASED V2G SCHEDULING

3.1 Problem formulation

In this research, the energy conversion strategy aims to save the customer's energy usage expenses while minimizing customer dissatisfaction, mitigating the power fluctuations on main grid due to the usage of residential PV as well as avoiding LIB thermal runaway caused by excessive heat generation. To this end, the cost function can be established as follows:

$$J_i = C_{e,i} + C_{b,i} + \omega_1 P_{dissa,i} + \omega_2 P_{grid,i} + \omega_3 P_{safe,i} \quad (19)$$

where ω_1 , ω_2 and ω_3 are the user-defined weights describing the importance of different targets, including the customer dissatisfaction, the power fluctuations, and the LIB operation safety, respectively. C_e is the electricity tariffs. C_b denotes the LIB degradation cost as:

$$C_{b,i} = \rho \cdot \Delta SOH \quad (20)$$

where ρ is the replacement cost coefficient of battery modules. P_{dissa} is the customer dissatisfaction calculated by Eq. (1). P_{grid} is the power fluctuations on main grid:

$$P_{grid,i} = P_{load,i} + P_{v2g,i} - P_{solar,i} \quad (21)$$

where $P_{v2g,i}$ is the converted power, $P_{load,i}$ is the domestic load and $P_{solar,i}$ is the power generated by solar PV.

Furthermore, the temperature of LIB needs to be constrained to avoid thermal runaway. On this basis, the penalty term is adopted to address these constraints. Correspondingly, the operation safety is evaluated as:

$$P_{safe,i} = \tau_1 P_{volt,i} + \tau_2 P_{temp,i} + \tau_3 P_{smooth,i} \quad (22)$$

where τ is weighing factor, $P_{volt,i}$, $P_{temp,i}$ and $P_{smooth,i}$ correspond to the voltage constraints, temperature constraint and the fluctuation of current respectively:

$$P_{volt,i} = \begin{cases} 0 & V_{min} \leq V_i \leq V_{max} \\ 1 & \text{other} \end{cases}, P_{temp,i} = \begin{cases} 0 & T_{c,min} \leq T_{c,i} \leq T_{c,max} \\ 1 & \text{other} \end{cases} \quad (23)$$

$$P_{smooth,i} = |I_i - I_{i-1}| \quad (24)$$

3.2 SAC DRL-based V2G scheduling

For the above multi-objective optimization problem, the deep reinforcement learning (DRL) method is adopted owing to the remarkable performance on the

ccc soft constraint optimization problem, as shown in Fig.3. In this study, the state space can be described as:

$$s = \{\text{SOC}_i, V_{t,i}, T_{c,i}, P_{\text{load},pre,i}, P_{\text{solar},pre,i}, C_{e,pre,i}\} \quad (25)$$

where SOC is the SOC of battery system, which are be obtained by on-board BMS using collected operating data of LIBs. V_t is the measured terminal voltage. $P_{\text{load},pre}$, $P_{\text{solar},pre}$ and $P_{e,pre}$ represent the predictive or prior knowledge in terms of domestic loads, generated solar power and electricity tariffs. And the reward function can be alternatively written according to Eq. (23):

$$\varphi(s, a) = \tanh(\sigma / J_i) \quad (26)$$

where σ is a constant which is set to coordinate the tangent function. The action space can be described as:

$$a = \{I^{2g} | I^{2g} \in [I_{dis}^{\min}, I_{ch}^{\max}]\} \quad (27)$$

In each iteration of scheduling process, the optimal current is selected by as the action of agent. As introduced above. Furthermore, the reward function can be used to evaluate the quality of each action based on the response of the environment, and finally the state of agent can be updated to s' . The agent explores the action space freely during training process, and the system state transfer process (a_i, s_i, r_i, s_{i+1}) is stored in an experience pool. The effectiveness of the strategy can be measured by the original value function as follows[11]:

$$Q_{\text{origin}}(S_i, \delta_i) = \varphi_i + \gamma E_{s_{i+1}, \delta_{i+1}} [Q(S_{i+1}, \delta_{i+1})] \quad (28)$$

where s_i , a_i , and φ_i are the state, action, and one-step reward in relation to step i . s_{i+1} and δ_{i+1} are the state and action after state transition, respectively. Moreover, γ is the discount factor and E is mathematical expectation. The value function can be established as:

$$Q_{\text{origin}}(S_i, \delta_i) = \varphi_i + \gamma E_{s_{i+1}, \delta_{i+1}} [Q(S_{i+1}, \delta_{i+1}) - \alpha \log(\pi_\phi(\delta_{i+1} | S_{i+1}))] \quad (29)$$

where α represents adjusting factor, π_ϕ is the obtained policy and ϕ is the corresponding distribution. And the Kullback-Leibler (KL) divergence-based information projection can be used to determine the policy function:

$$\Pi = \arg \min D_{KL}(\pi_\phi(\cdot | S_i) || \frac{\exp(Q(S_i, \cdot) / \alpha)}{Z(S_i)}) \quad (30)$$

where Π is the feasible sets of policy function, $D_{KL}(\cdot)$ is the KL divergence, $Z(S_i)$ is the logarithm partition function.

The policy network π and the value network Q are built using two deep neural networks (DNNs). Moreover, to reduce unsteady iteration during model training, the target networks Q' is used. The data during state transition is kept in the experience pool since the experience replay buffer $D_i = [s_i, \delta_i, \varphi_i, s_{i+1}]$ is used to update the value network as:

$$J_Q(\theta^Q) = E_{[s_i, \delta_i, \varphi_i, s_{i+1}]D} \cdot \frac{1}{2} [Q(s_i, \delta_i) - (\varphi_i + \gamma(Q'(s_{i+1}, \pi_\phi(s_{i+1})) - \alpha \log(\pi(\delta_{i+1} | s_{i+1}))))]^2 \quad (31)$$

Then the soft update can be realized as follows:

$$\theta^Q \leftarrow (1 - \tau)\theta^Q + \tau\theta^Q \quad (32)$$

where τ represents the step factor for updating.

Then the policy network can be updated as follows:

$$J_\pi(\theta^\phi) = D_{KL}(\pi_\phi(\cdot | s_{i+1}) || \exp(\frac{1}{\alpha} Q(s_i, \cdot) - \log Z(s_i))) \quad (33)$$

$$= E_{s_i, D} [\log \pi_\phi(\delta_i | s_i) - \frac{1}{\alpha} Q(s_i, \pi_\phi(s_i)) + \log Z(s_i)]$$

In the initial training stage, the SAC algorithm selects the action stochastically from the experience buffer. And the DRL agent can investigate options in the direction of optimality benefited by the stochastic character of SAC to improve the training efficiency. Moreover, the abbreviation of adaptive motion (ADAM) algorithm is used for parameters optimization in DNNs.

3.3 Method Implementation in cyber-physical system

The above DRL-based method can be considered as two distinct procedures, i.e., the offline training and online scheduling. Correspondingly, the established method is implemented based on the CPS framework due to its separable feature. A feasible arrangement is that the model is first trained in the cyber layer-cloud server, whereafter are downloaded to the onboard controllers located in the physical layer to perform the real-time scheduling, as shown as Fig. 1.

4. CASE STUDIES

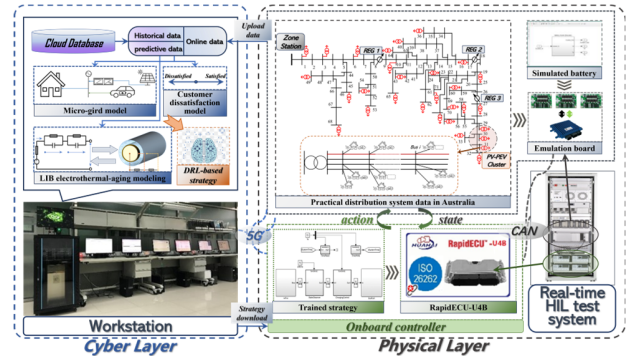


Fig. 4 Diagram of the testing system

4.1 Conditions for validation

The scheduling test is performed on the hardware-in-loop (HIL) platform shown in Fig.4 in this study to verify the comprehensive performance of the proposed strategy. To this end, a distribution network taken from a New South Wales distribution system in Australia is studied in this paper, comprising low voltage (LV) and medium voltage (MV) feeders[12]. There are more than 70 11 kV nodes in the 80 km long rural network. Specifications of the LV feeder in this study are as shown in Table I. To analyze the effects of PV and PEV, the customers on the LV feeders connected to buses 29, 30, and 31 have a cluster with rooftop PV and PEVs. The load profile data, the PV data corresponds to a PV output profile and the electricity tariffs throughout a single day

are obtained from an Australian distribution utility and the Commonwealth Scientific and Industrial Research Organizations. TESLA Model S is adopted as the simulated PEV. The specifications are as shown in Table II. The minimum SOC of the on-board battery in PEVs is determined according to a 30 km per day travel assumption based on the driving habit statistics in [13]. Moreover, the trained strategy is downloaded into an onboard controller in the HIL platform for real-time scheduling. The interactive process between the onboard controller and the environment simulator is coordinated by a real-time PC.

TABLE I Specifications of a Low voltage feeder

Feeder Length	240
MV/LV Transformer	160kVA, 3ph
Maximum Load per Customer	2.2 kW at 0.95 PF (lag)
PV Size	4kW

TABLE II Specifications of studied PEVs

PEV make and model	Tesla Model S
Battery type	18650 Lithium Ion Battery
Number of cells	7104 (16×6×74)
Charger efficiency	0.95

4.2 Result analysis

In this study, the proposed method is compared with a rule-based one [2] and an optimization-based one [5] respectively to verify the performance in terms of fluctuation mitigation, charging cost, customer service quality and battery operation safety.

For the PV mitigation, the domestic load and PV output power in a PV-PEV cluster is as shown in Fig. 5(a). The voltage profile at the LV side of an MV/LV substation transformer and the effect of PEV on voltage rise mitigation during midday is shown in Fig. 5(b). Obviously, the voltage is steadier in the proposed method compared to the two traditional methods due to the ability to update charging strategies dynamically in response to changes in environmental conditions.

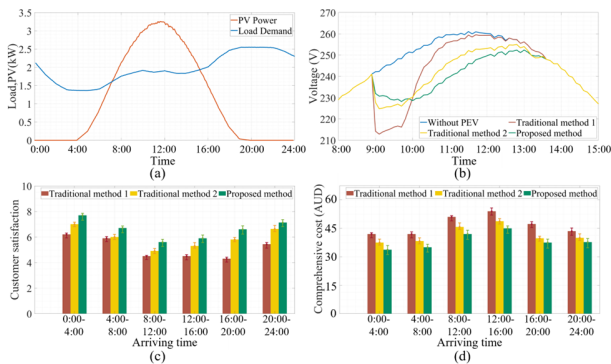


Fig. 5 The results of verification on (b) PV impact mitigation; (c) charging satisfaction; (d) cost

Additionally, the effects of reaching time on the customer satisfaction and the comprehensive charging cost are verified. Customer satisfaction in the controlled

charging mode is defined as the uncontrolled satisfaction level $T_{hd} - (T_{rh} + L_{cd}) + 1$ minus the calculated customer dissatisfaction in Eq. (1). As shown in Fig. 5(c) and (d), due to the impact of electricity tariff at different time periods and other optimization goals, customers' satisfaction when charging during midday is lower than those during early morning and evening. Similarly, the comprehensive cost when charging during midday is also higher than those in other periods. Nevertheless, the proposed method consistently outperforms the two traditional methods in optimizing both customer satisfaction and charging costs at all times.

As shown in Fig. 6 (a)-(c), for the proposed method, the charging current begins at a high C-rate to hasten the charging process because none of the limitation is engaged during this period. As the charging process continues, the temperature and voltage limitations are sequentially imposed, forcing the charging current to drop. By contrast, in the two traditional methods, the charging strategy cannot make timely and accurate adjustments to temperature and voltage changes, resulting in temperatures exceeding the set threshold, threatening the operational safety and useful life of LIBs.

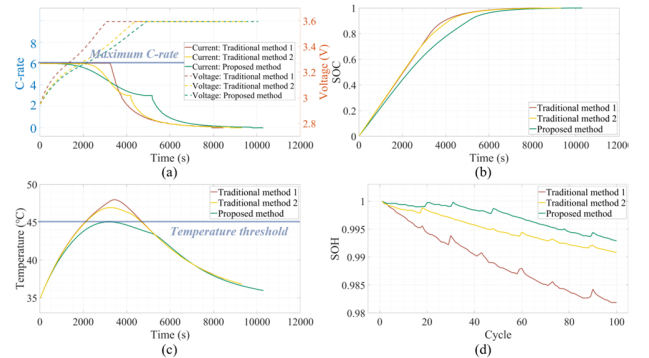


Fig. 6 Results of simulated and practical battery tests

After that, the testing is carried out with the platform in Fig. 4 while the only difference is that the battery simulator is replaced with practical battery. Three practical battery cells are tested in the same scenario (ambient temperature = 35°C) using different methods, respectively. After each charging/discharging cycle, the SOH of each cell can be obtained using the estimation method in [14]. The results are shown in Fig. 6(d), the capacity deterioration rate (100 cycles) is decreased by 69% and 23% compared to the two traditional methods.

5. CONCLUSION

A novel knowledge-based charging scheduling method is developed for PEVs in this article to mitigate solar PV impact while minimize the expected customer's charging cost, including energy cost and battery aging cost as well as satisfying the customer service quality and ensuring battery operation safety. The overtemperature

penalty and aging cost in V2G scheduling was analyzed and quantified based on an electrothermal-aging model and included in the optimization target alongside the voltage fluctuation at the LV side of an MV/LV substation transformer and the consumer satisfaction evaluated by a Kano's model. On this basis, an up-to-date DRL algorithm was adopted to assess the V2G scheduling behavior intelligently with great superiority on convergence speed and optimizing performance. The proposed strategy is further performed within a cyber physical system-based framework, where the complicated training is carried out in the cloud, while the trained low-complexity policy is executed in the onboard controller to mitigate high computing burden. The proposed strategy is verified by comparing with two traditional methods in a hardware-in-Loop test and practical battery charging/discharging experiments combined by a real distribution system in Australia. The result shows that benefiting by an active combination of SAC-DRL algorithm and the assisted models, the voltage increase at medium/low voltage substation transformers can be effectively restricted to a maximum of 30V during the PV generated power peak period while the customer dissatisfaction and charging cost can be reduced by over 10% and 15% respectively compared to the reference methods. Simultaneously, the degradation rate of LIB can be reduced by over 23% while maintaining internal temperature of LIB lower than the safety threshold.

DECLARATION OF INTEREST STATEMENT

The authors declare that they have no known competing financial interests or personal relationships that could have appeared to influence the work reported in this paper. All authors read and approved the final manuscript.

REFERENCE

[1] Yue H, He H, Han M, Gong S. Active disturbance rejection control strategy for PEMFC oxygen excess ratio based on adaptive internal state estimation using unscented Kalman filter. *Fuel*. 2024;356.

[2] Sah B, Kumar P, Bose SK. A Fuzzy Logic and Artificial Neural Network-Based Intelligent Controller for a Vehicle-to-Grid System. *Ieee Systems Journal*. 2021;15:3301-11.

[3] Nimalsiri NI, Ratnam EL, Smith DB, Mediawathe CP, Halgamuge SK. Coordinated Charge and Discharge Scheduling of Electric Vehicles for Load Curve Shaping. *Ieee Transactions on Intelligent Transportation Systems*. 2022;23:7653-65.

[4] Ghofrani M, Arabali A, Etezadi-Amoli M, Fadali MS. Smart Scheduling and Cost-Benefit Analysis of Grid-Enabled Electric Vehicles for Wind Power Integration. *Ieee Transactions on Smart Grid*. 2014;5:2306-13.

[5] Ebrahimi M, Rastegar M, Mohammadi M, Palomino A, Parvania M. Stochastic Charging Optimization of V2G-Capable PEVs: A Comprehensive Model for Battery Aging and Customer

Service Quality. *Ieee Transactions on Transportation Electrification*. 2020;6:1026-34.

[6] Huang RC, He HW, Zhao XY, Wang YL, Li ML. Battery health-aware and naturalistic data-driven energy management for hybrid electric bus based on TD3 deep reinforcement learning algorithm. *Applied Energy*. 2022;321.

[7] Feng YX, Hu BT, Hao H, Gao YC, Li ZW, Tan JR. Design of Distributed Cyber-Physical Systems for Connected and Automated Vehicles With Implementing Methodologies. *Ieee Transactions on Industrial Informatics*. 2018;14:4200-11.

[8] Kirgizov UA, Kwak C. How can a quantitative analysis of Kano's model be improved further for better understanding of customer needs? *Total Quality Management & Business Excellence*. 2022;33:1605-24.

[9] Zhang C, Li K, Deng J. Real-time estimation of battery internal temperature based on a simplified thermoelectric model. *Journal of Power Sources*. 2016;302:146-54.

[10] Ebbesen S, Elbert P, Guzzella L. Battery State-of-Health Perceptive Energy Management for Hybrid Electric Vehicles. *Ieee Transactions on Vehicular Technology*. 2012;61:2893-900.

[11] Wu JD, Wei ZB, Li WH, Wang Y, Li YW, Sauer DU. Battery Thermal- and Health-Constrained Energy Management for Hybrid Electric Bus Based on Soft Actor-Critic DRL Algorithm. *Ieee Transactions on Industrial Informatics*. 2021;17:3751-61.

[12] Alam MJE, Muttaqi KM, Sutanto D. Effective Utilization of Available PEV Battery Capacity for Mitigation of Solar PV Impact and Grid Support With Integrated V2G Functionality. *Ieee Transactions on Smart Grid*. 2016;7:1562-71.

[13] Taylor J, Smith JW, Dugan R, Ieee. Distribution Modeling Requirements for Integration of PV, PEV, and Storage in a Smart Grid Environment. General Meeting of the IEEE-Power-and-Energy-Society (PES). Detroit, MI2011.

[14] Zhao XY, He HW, Li JW, Wei ZB, Huang RC, Shi M. From Grayscale Image to Battery Aging Awareness-A New Battery Capacity Estimation Model With Computer Vision Approach. *Ieee Transactions on Industrial Informatics*. 2023;19:8965-75.